IEEE Access
Multidisciplinary ⋮ Rapid Review ⋮ Open Access Journal

Received 13 January 2024, accepted 13 February 2024, date of publication 19 February 2024, date of current version 26 February 2024.

Digital Object Identifier 10.1109/ACCESS.2024.3366931

RESEARCH ARTICLE

A Comparison Analysis of a New Switched-Inductor and Conventional Split Source Inverter Structures

MOHAMED A. ISMEIL[1], (Member, IEEE), AHMED ABDELALEEM[1], AHMED ISMAIL M. ALI[1], (Member, IEEE), M. NASRALLAH[1], HANY S. HUSSEIN[2], (Senior Member, IEEE), AND ESSAM E. M. MOHAMED[1], (Member, IEEE)

[1]Electrical Engineering Department, Faculty of Engineering, South Valley University, Qena 83523, Egypt
[2]Electrical Engineering Department, Faculty of Engineering, King Khalid University, Abha 61411, Saudi Arabia

Corresponding author: Ahmed Abdelaleem (ahmed.abdelaleem@eng.svu.edu.eg)

This work was supported by the Deanship of Scientific Research at King Khalid University through a Large Group Research Project under Grant RGP2/179/44.

ABSTRACT Several impedance source converters are receiving more attention currently due to their bucking-boosting capability in a single conversion step, reduced system cost, size, footprint, and control system complexity compared to dual-stage structures. This paper introduces a comparative analysis of a recent Split Source Inverter (SSI) topology and one of its modified versions which is called Switched-inductor Split Source Inverter (SL-SSI). Obviously, the SSI structure advances many features compared to the conventional Z-Source (ZSI), and quasi-Z-Source Inverters (qZSI) such as minimized component voltage and current stress for single-stage voltage boosting properties. In addition, the mathematical modulation of the SSI and SL-SSI are analyzed for inverter power elements design and selection strategy, and control system simplification. The theoretical operation of the two topologies is investigated and analyzed considering the Sinusoidal Pulse-width Modulation (SPWM) strategy. The SSI and SL-SSI are designed for 10 kW system ratings and implemented using Opal RT OP5410.

INDEX TERMS Voltage source inverter (VSI), single-stage converter, split source inverter (SSI), switched-inductor (SL).

NOMENCLATURE

SSI	Split Source Inverter.
SL-SSI	Switched-inductor Split Source Inverter.
ZSI	Z-source Inverter.
qZSI	quasi-Z-Source Inverter.
SPWM	Sinusoidal Pulse-width Modulation.
VSI	Voltage Source Inverter.
DC-L-C	DC-link Capacitor.
SDSI	Split Delta Source Inverter.
ASSI	Active Split Source Inverter.
THD	Total Harmonic Distortion.

The associate editor coordinating the review of this manuscript and approving it for publication was Zhilei Yao.

I. INTRODUCTION

Power electronics converters are essential components in facilitating the power conversion process, where their beneficial characteristics make them highly required to replace earlier systems. Moreover, considering the significance of renewable energy, several studies have concentrated on renewable system converters [1]. The most popular DC-AC power converters used in power electronic systems are Voltage Source Inverters (VSIs) [2], [3]. However, voltage buck capability is only considered in the VSI with the inversion stage. Numerous applications utilizing high DC rails do not exhibit any issues at this juncture. A recommendation exists that the AC output voltage should transcend the DC input voltage. Consequently, in these scenarios, an additional boosting stage is necessary [4], [5]. However, using a separate

DC-DC boost converter necessitates a second switching device, which augments the system's overall footprint and cost, and reduces its efficiency. Due to its advantages over the dual-stage counterpart in respect of cost, volume, weight, and system intricacy, there has been growing interest in DC-AC power converters that integrate buck-boost functionality within a single-stage operation [6], [7], [8]. Various impedance-based inverter structures are presented in this respect).) [9], [10]. The conventional design of a Z-source inverter (ZSI) is the dominant topology within this class of power converters [11], [12]. A new configuration derived from the Z-source inverter is referred to as the quasi ZSI (qZSI) [13], [14]. Nevertheless, these configurations come with certain drawbacks, including discontinuous input DC current and DC-link Voltage. Furthermore, as the voltage gain increases, there is a corresponding rise in voltage stress. Additionally, the need for extra shoot-through states to achieve boosting purposes can complicate the controller design.

In recent developments, alternative Split Source Inverter (SSI) setups have been introduced for both three-phase [15], [16] and single-phase applications [17]. These configurations include the standard VSI along with a boosting inductor and a DC-link Capacitor (DC-L-C), as illustrated in Fig. 1 for the three-phase design and Fig. 2 for the single-phase variant. The SSI concept relies on a sequential process: first, the boosting inductor is charged using the input source, then the DC-L-C is charged using both the input source and the boosting inductor. Subsequently, the VSI converts the elevated DC voltage into AC power. Also, the SSI configuration exhibits numerous enhancements compared to ZSI and qZSI, including reduced reliance on passive components, sustained input current, consistent DC-link voltage, the need for only eight states like the conventional VSI, thus eliminating the requirement for shoot-through states, and its ability to function with any modulation technique.

The SSI has been adapted to function as a three-level inverter by incorporating a flying capacitor bridge, aimed at reducing voltage stress on the switches [18], [19], and also by using the diode clamped bridge [20]. The MOSFET was initially employed in the single-phase SSI as described in [21], later undergoing modifications to reduce the number of switching devices, as discussed in [22]. Subsequently, it found application in a standalone PV system, as detailed in [23]. In [17] a different structure has been represented, where it is conceivable to utilize a common-cathode dual-diode package instead of two separate diodes to reduce parasitic inductance in the commutation track of these diodes, furthermore, the difficulty of high-frequency commutation in these input diodes has been solved. Another structure, which is called Active SSI (ASSI), is presented in [24], It substitutes the two clamping diodes in SSI with reverse-blocking switches, resulting in more controllability in the topology. Another topology derived from the SSI is identified as Split Delta Source Inverter (SDSI) [25], which aims to enhance the DC voltage gain. In [26], a switched-inductor is employed in conjunction with the SSI to achieve the boosting function, and the switched-inductor-capacitor is implemented in [27].

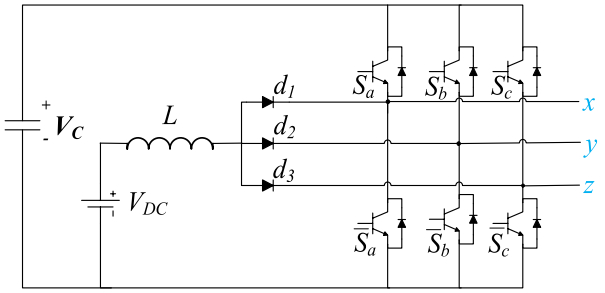

FIGURE 1. Three-phase split source inverter (SSI).

This paper seeks to investigate the conventional SSI and modified SL-SSI inverter structures considering a 10kW system power rating with implementing Sinusoidal Pulse-Width Modulation (SPWM). In addition, the mathematical modeling of the proposed systems has been investigated for inverter components design, after illustrating the modulating operation of both structures. The number of passive components, the operating manner, the design specifications, and the power quality are the main objectives of the comparison discussion. Moreover, the efficiency and power loss distribution of the SL-SSI have been compared with the conventional SSI under output power variations. Hence, the paper highlights can be summarized as follows;

- Studying and investigating conventional SSI compared to the SL-SSI considering the same power ratings (10kW).
- Mathematical modelling of the SSI and SL-SSI structures.
- Power loss contribution and efficiency of both converters are conveyed.
- A comparative analysis of the SL-SSI and SSI has been established.

The following is how this paper is structured: part II indicates the operation, design, and results of a 10 kW SSI system, part III indicates the operation, design, and results of a 10 kW SL-SSI system, part IV points to the power loss calculation of both configurations, part V shows a comparative study, then the conclusion. The systems are validated using the real-time device Opal-RT OP4510.

II. THREE-PHASE SPLIT SOURCE INVERTER

A. OPERATION

The conventional structure is as depicted in Fig. 1, the DC source is connected to the three-phase bridge inverter via an inductor and three diodes. Also, the DC-L-C is connected in parallel with the three-phase bridge. The SSI inverter configuration is similar to the VSI and considers eight operational states as described in TABLE. 1 and depicted in Fig. 3. The input source charges the inductor when any of the lower switches is ON-stated as depicted in Fig. 3.1-7. Obviously, both the input source and the inductor charge the DC-L-C when all the upper switches are ON-stated simultaneously

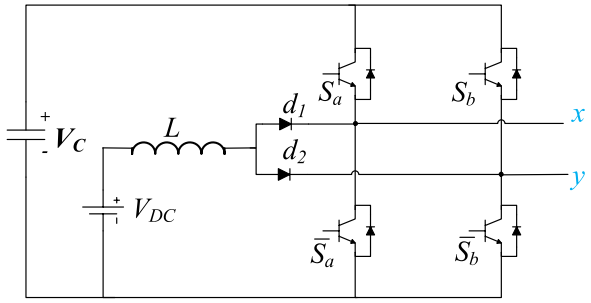

FIGURE 2. Single-phase split source inverter (SSI).

as depicted in Fig. 3.8. Therefore, the DC input voltage is boosted and then converted to AC by the H-bridge circuit. One of the main advantages of the SSI is that it can be used with any modulation scheme. In this paper, the SSI inverter is investigated and tested using SPWM as depicted in Fig. 4.

B. SSI INVERTER'S MATHEMATICAL MODELLING

The inductor L of the SSI inverter is charged with a duty cycle of D, that can be mathematically expressed as follows,

$$D = \frac{t_x}{t_x + t_y} \tag{1}$$

where, t_x is the inductor charging time and t_y is the discharging time. The minimum duty cycle D_{min} can be delivered from,

$$D_{min} = \frac{1}{4}M + \frac{1}{2} \tag{2}$$

where, M is the modulation index, the maximum Duty cycle D_{max} can be delivered from,

$$D_{max} = \frac{1}{2}M + \frac{1}{2} \tag{3}$$

The average duty cycle D_{avg} can be represented as follows,

$$D_{avg} = \frac{3\sqrt{3}}{4\pi}M + \frac{1}{2} \tag{4}$$

During the charging period, the inductor voltage V_L equals

$$V_L = V_{DC} \tag{5}$$

where, V_{DC} is the input DC voltage.

During the discharge period,

$$V_L = V_{DC} - V_C \tag{6}$$

where, V_C is the DC-LC voltage.

By applying the inductor voltage balance,

$$D \cdot V_{DC} + (1 - D)(V_{DC} - V_C) = 0 \tag{7}$$

Hence,

$$V_C = \frac{V_{DC}}{1 - D} \tag{8}$$

Therefore, the SSI inverter boosting factor B can be formulated as follows,

$$B = \frac{1}{1 - D} \tag{9}$$

TABLE 1. States of the conventional three-phase SSI.

S_a, S_b, S_c	Inductor State	Fig. 3
(000)	Charge	1
(001)	Charge	2
(010)	Charge	3
(011)	Charge	4
(100)	Charge	5
(101)	Charge	6
(110)	Charge	7
(111)	Discharge	8

By substituting the average duty cycle in (8)

$$V_C = V_{DC} \cdot \frac{4\pi}{2\pi - 3\sqrt{3}M} \tag{10}$$

The peak of the output fundamental phase voltage V_{pp} can be indicated by,

$$V_{pp} = V_{DC} \cdot \frac{2\pi.M}{2\pi - 3\sqrt{3}M} \tag{11}$$

Therefore, the overall inverter voltage gain g can be indicated by

$$g = \frac{2\pi.M}{2\pi - 3\sqrt{3}M} \tag{12}$$

The required inductance L and capacitance C values can be indicated from [15],

$$L \approx \frac{D_{max}V_{DC}}{2f_c\Delta I_L} + \frac{KMV_C}{6\pi f_f \Delta I_L} \tag{13}$$

$$C \approx \frac{(1 - D_{min})I_L}{2f_c\Delta V_C} + \frac{KMI_L}{6\pi f_f \Delta V_C} \tag{14}$$

where, f_f and f_c are the fundamental and carrier frequency consecutively, ΔI_L is the inductor current ripple, and ΔV_C is the DC-L-C voltage ripple.

K is a constant, its value depends on the modulation technique, and it is equal to $\frac{3\sqrt{3}}{8\pi}$ for SPWM.

C. SYSTEM DESIGN

The SSI inverter design process for a 10.0 kW power rating is analyzed in this part of the paper. It is anticipated that the SSI inverter is supplied from a battery with a nominal voltage of 100V. TABLE 2 explains the design process. The inductor is chosen to be 8mH and the DC-L-C is chosen to be $120\mu F$, these values; which are determined using (13) and (14); depend on the acceptable and required current and voltage ripples in each element consequently. The design limitations for the inductor current and the DC-L-V voltage ripples are 20%, and 3%, respectively. The peak output voltage is considered as $220\sqrt{2}$V at a fundamental frequency of 50Hz, and the carrier frequency is 2.5 kHz. The output load is considered an RL load. The values of the modulation index, minimum, maximum, and average duty cycle; which

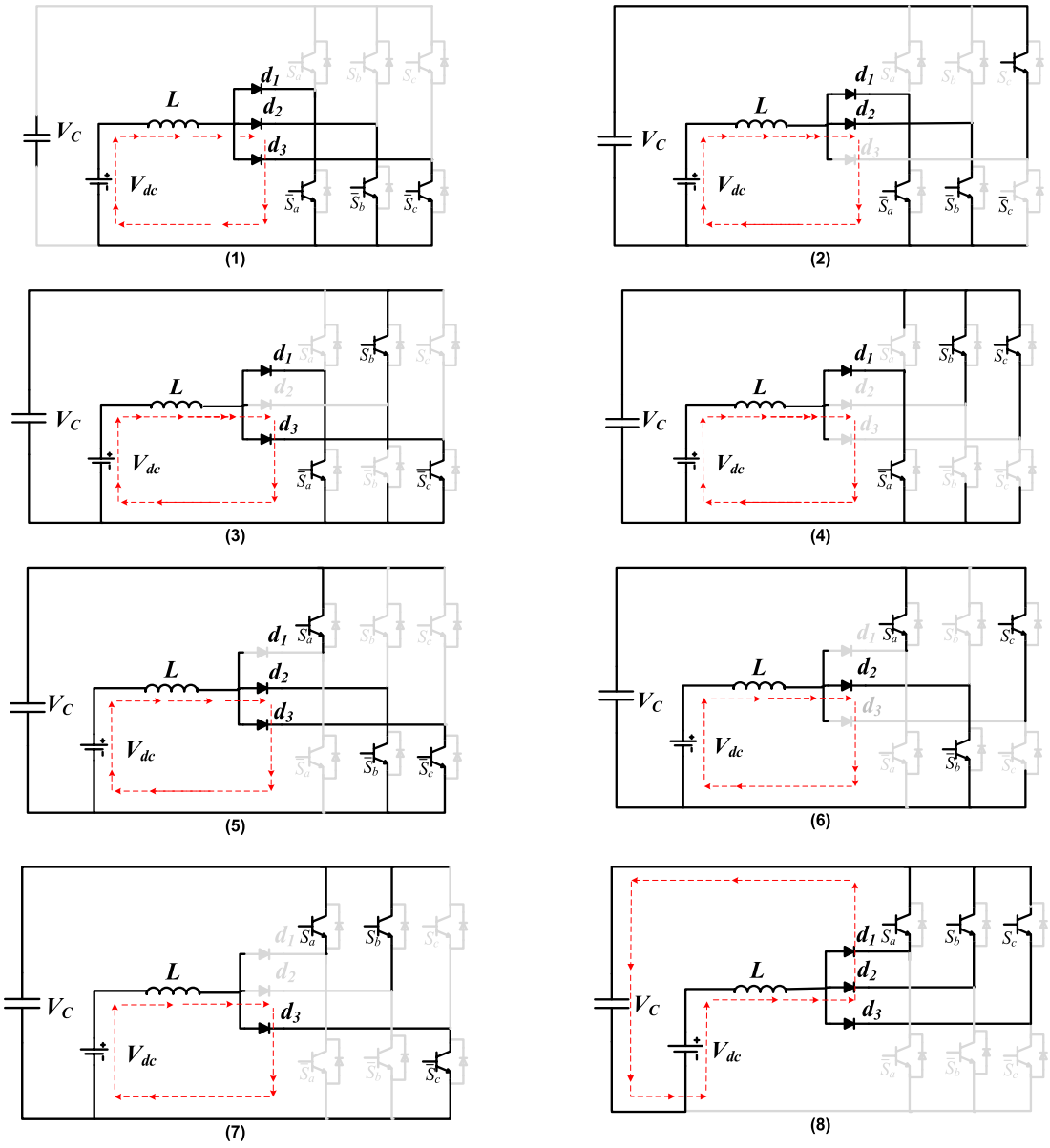

FIGURE 3. The switching states of three-phase SSI.

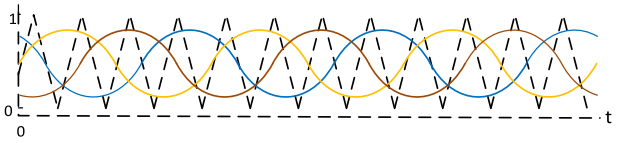

FIGURE 4. Sinusoidal pulse-width modulation (SPWM).

are determined using (1), (2), (3), and (4); are 0.8718, 0.7177, 0.9354, and 0.8708 respectively.

D. RESULTS

The system is validated using the Opal-RT device OP4510, The SPWM technique and the proposed converter are designed using MATLAB/Simulink, RT-LAB block sets, the host PC to OP4510 interface, real-time to Simulink sets and the OP4510 to oscilloscope interface, where Fig. 5 illustrates the system schematic and the system photograph has been depicted Fig. 6. Fig. 7 shows the input inductor current, where the zoomed part shows that the average value is 100 A with upper and lower peaks at 110 A and 90 A, consecutively, that coincide with the aforesaid current ripples limitations of 20%. Fig. 8 illustrates the DC-L-C voltage, where the mean value is approximately 714 V and fluctuates between 725 and 705 V. Obviously, the voltage ripples follow the system design limitations with 3% voltage ripples. Fig. 9 depicts the AC load current waveforms confirming the appropriate filter of the AC side for this structure. Fig. 10 shows the different harmonic orders (even harmonics) of the load current indicating the fundamental component and Total Harmonic Distortion (THD) in the output current. In addition, Fig. 11 depicts the SSI

TABLE 2. The design elements of a 10 kW SSI system.

Element	Symbol	Value	Equation
Input DC voltage	V_{DC}	100 V	..
Input inductor current	I_L	100 A	..
Peak output phase voltage	V_{pp}	$220\sqrt{2}$ V	..
Carrier frequency	f_c	2.5 kHz	..
Fundamental frequency	f_f	50 Hz	..
Modulation index	M	0.8708	(11)
DC-L-C voltage	V_C	714.6 V	(10)
Minimum duty cycle	D_{min}	0.7177	(2)
Maximum duty cycle	D_{max}	0.9354	(3)
Average duty cycle	D_{avg}	0.8708	(4)
The input inductor	L	8 mH	(13)
The DC-link capacitor	C	1200 μF	(14)

FIGURE 5. Real-time system block diagram.

system results, input inductor current, capacitor voltage, and the three-phase grid sinusoidal currents on the oscilloscope screen.

III. THREE-PHASE SWITCHED-INDUCTOR SPLIT SOURCE INVERTER

A. OPERATION

The switched-inductor is utilized with a lot of inverter topologies for increasing the DC voltage gain as with ZSI in [28], [29], and [30], with qZSI in [31], and [32], and with SSI [26]. The conventional inductor is replaced with a switched-inductor in the modified Switched-Inductor Split Source Inverter (SL-SSI) architecture, as depicted in Fig. 12.

The switched-inductor differs from the conventional inductor by its two different states, the first is that the two included inductors are connected in parallel when the diodes d_a, d_b are forward-biased and d_c is reverse-biased, the second state is that the two inductors are connected in series when the diodes d_a, d_b are reverse-biased and d_c is forward-biased. The operating behavior of the switched-inductor can be used with single-stage inverters to increase the DC boosting gain.

As mentioned before the SSI has two main switching states, charging and discharging, the same occurs in SL-SSI. TABLE. 3 and Fig. 12 describe the switching states in detail. When any of the lower switches is ON-stated the input source charges the switched-inductor which acts as two parallel inductors to decrease the overall inductance as depicted from Fig. 13a to Fig. 13g, when all upper switches are ON-stated simultaneously the input source and the switched-inductor charge the DC-L-C, in this state the switched-inductor acts

FIGURE 6. The system using Opal RT OP4510.

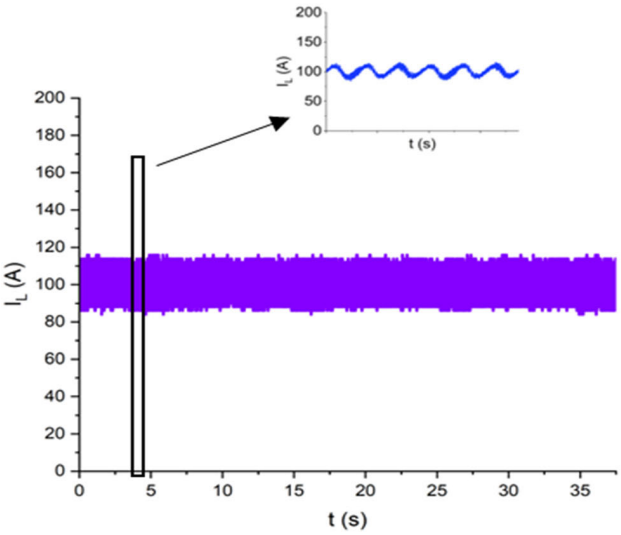

FIGURE 7. The input inductor current of the 10 *kW* SSI system.

as two series inductor to increase the overall inductance, and the charging level consequently as shown in Fig. 13h.

As SSI, SL-SSI can be used with any modulation scheme. In this paper, SL-SSI is examined with SPWM.

B. MATHEMATICAL DERIVATION

SL-SSI has the same maximum, minimum, and average duty cycle as in SSI, which are mentioned in (2), (3), and (4). The main difference is that during the charging period,

$$V_{L_a} = V_{L_b} = V = V_{DC} \tag{15}$$

where, V_{L_a}, and V_{L_b} are the inductors L_a and L_b voltage. During the discharge period,

$$V_{L_a} + V_{L_b} = 2V = V_{DC} - V_C \tag{16}$$

When implementing the inductor voltage balance,

$$D \cdot V_{DC} + \frac{1}{2} \cdot (1 - D)\,(V_{DC} - V_C) = 0 \tag{17}$$

Hence,

$$V_C = \frac{1 + D}{1 - D} \cdot V_{DC} \tag{18}$$

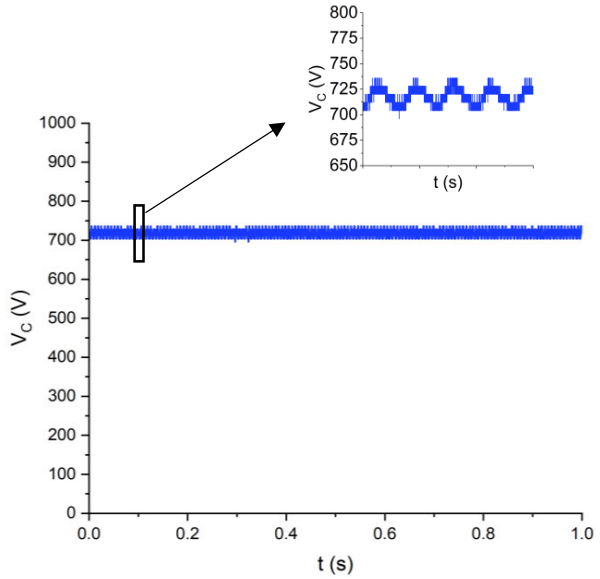

FIGURE 8. The DC-L-C voltage of the 10 *kW* SSI system.

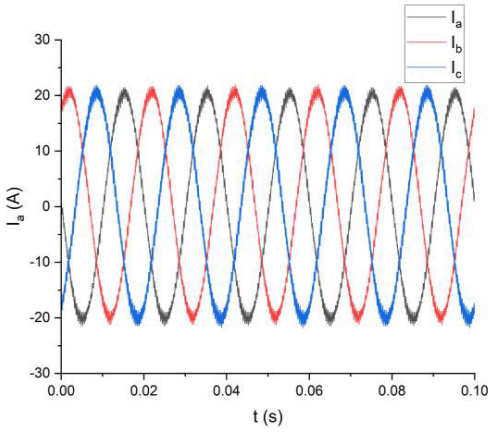

FIGURE 9. The three-phase output current waveforms of the 10 kW SSI system.

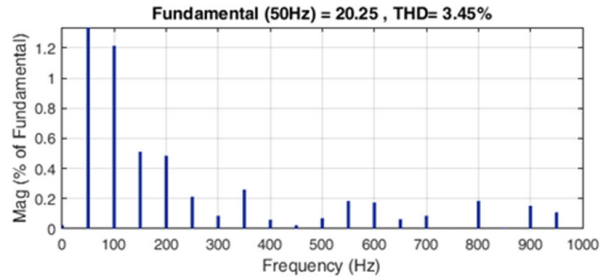

FIGURE 10. The total harmonic distortion (THD) of the output phase current of 10 kW SSI system.

Hence, the boosting factor B_{SL}

$$B_{SL} = \frac{1+D}{1-D} \tag{19}$$

When comparing B_{SL} with the boosting factor in SSI in (9), this clarifies the increase in the boosting factor as depicted in Fig. 14.

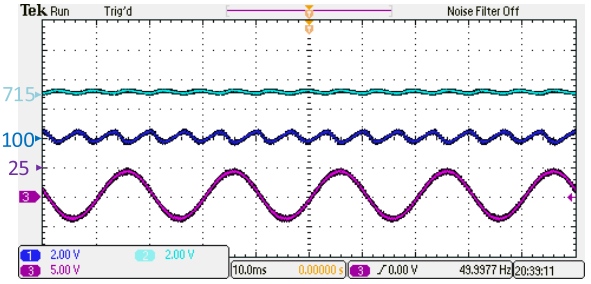

FIGURE 11. The oscilloscope screen photograph of the 10 *kW* SSI system.

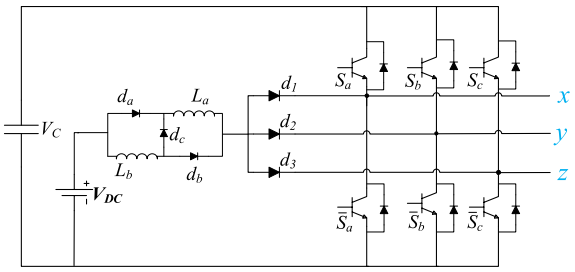

FIGURE 12. Three-phase switched-inductor SSI (SL-SSI).

By substituting the average duty cycle in (18)

$$V_C = V_{DC} \cdot \frac{6\pi + 3\sqrt{3}M}{2\pi - 3\sqrt{3}M} \tag{20}$$

The peak of the output fundamental phase voltage V_{pp} can be indicated from

$$V_{pp} = V_{DC} \cdot \frac{M}{2} \cdot \frac{6\pi + 3\sqrt{3}M}{2\pi - 3\sqrt{3}M} \tag{21}$$

Therefore, the overall inverter gain g_{SL} can thus be indicated from,

$$g_{SL} = \frac{M}{2} \cdot \frac{6\pi + 3\sqrt{3}M}{2\pi - 3\sqrt{3}M} \tag{22}$$

The desired inductance L_a, L_b and capacitance C magnitudes can be indicated from [26],

$$L_a = L_b \approx \frac{D_{max} V_{DC}}{4 f_c \Delta I_L} + \frac{KMV_C}{12\pi f_f \Delta I_L} \tag{23}$$

$$C \approx \frac{(1 - D_{min}) I_{DC}}{4 f_c \Delta V_C} + \frac{KMI_{DC}}{12\pi f_f \Delta V_C} \tag{24}$$

where, I_{DC} is the input DC current and ΔI_L is the ripple in the inductor current.

C. SYSTEM DESIGN

The SL-SSI inverter design process for a 10.0kW power rating is analyzed in this part of the paper. The SL-SSI is designed to be powered by a battery with a nominal voltage of 50 V. The design process is described in TABLE 4. Thus, the SL-SSI's inductors and capacitor are selected based on the required current and voltage ripples in each element. The inductor current ripple is limited to 20%, while the capacitor voltage ripple is limited to 3%. After using (23) and (24), the chosen inductor values are 3.5 mH, and the

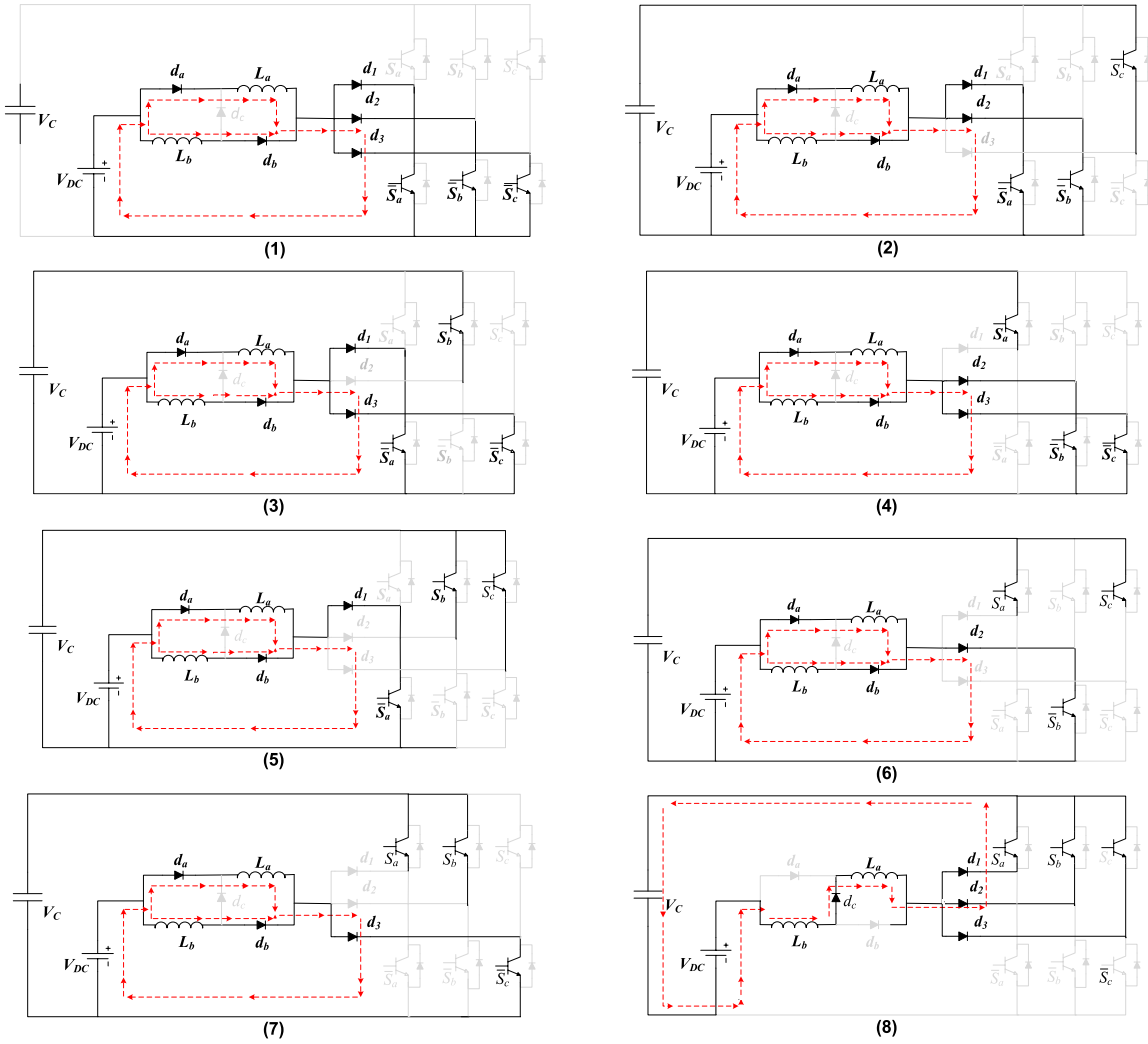

FIGURE 13. The operational states of three-phase SSI.

TABLE 3. The operational states of the SL-SSI.

State	Capacitor State	Switched-inductor		Fig. 13
		L_a	L_b	
(000)	Discharge	Charge	Charge	1
(001)	Discharge	Charge	Charge	2
(010)	Discharge	Charge	Charge	3
(011)	Discharge	Charge	Charge	4
(100)	Discharge	Charge	Charge	5
(101)	Discharge	Charge	Charge	6
(110)	Discharge	Charge	Charge	7
(111)	Charge	Discharge	Discharge	8

chosen capacitor value is 1200μF. The peak output voltage is considered as $220\sqrt{2}$V, the fundamental frequency is chosen as 50Hz, and the carrier frequency is chosen as 2.5 kHz. The output load is considered an *RL* load. The determined values of the modulation index, minimum, maximum, and average duty cycle are 0.8873, 0.7218, 0.9437, and 0.8669 respectively.

D. RESULTS

This section shows the verification of the SL-SSI inverter system, where Fig. 15 displays the current waveform through a single inductor. Obviously, it validates the inductor design limitations with a 20% current ripple. Fig. 16 displays the capacitor voltage, where the average value equals approximately 701 *V* and fluctuations are between 710 and 609 *V* considering peak-to-peak voltage ripples of 2.5%, which follows the passive elements design limitations. Fig. 17 shows the three-phase output sinusoidal current waveforms, which exhibit reduced THD sinusoidal current waveforms compared to SSI, with lower high-frequency oscillation that mitigates the requirements for a rigidly and high-cost designed filter at the AC side. Fig. 18 shows the different harmonic orders (even harmonics) of the load current waveforms indicating the fundamental component and THD of the output current. Similarly, Fig. 19 depicts the inductor current,

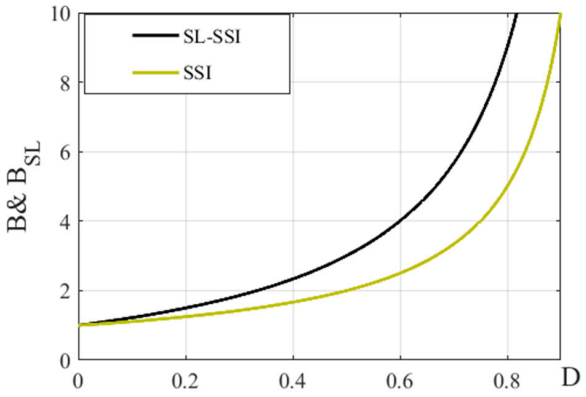

FIGURE 14. The difference between the boosting factor in SSI & SLSSI.

TABLE 4. The design elements of a 10 KW SL-SSI system.

Element	Symbol	Value	Equation
Input DC voltage	V_{DC}	50 V	..
Input current	I_L	200 A	..
Peak output phase voltage	V_{pp}	$220\sqrt{2}$ V	..
Carrier frequency	f_c	2.5 kHz	..
Fundamental frequency	f_f	50 Hz	..
Modulation index	M	0.8873	(21)
DC-link voltage	V_C	701.3 V	(20)
Minimum duty cycle	D_{min}	0.7218	(2)
Maximum duty cycle	D_{max}	0.9437	(3)
Average duty cycle	D_{avg}	0.8669	(4)
The first inductor	L_a	3.5 mH	(23)
The second inductor	L_b	3.5 mH	(23)
The DC-link capacitor	C	1200 μF	(24)

capacitor voltage, and three-phase load current waveforms captured on the oscilloscope screen.

IV. POWER LOSS MODEL OF SSI & SL-SSI

The losses incurred by the switches in a converter primarily consist of conduction and switching losses. At lower switching frequencies, conduction losses take precedence. Conversely, at higher switching frequencies, switching losses become more significant. In the case of an IGBT with an anti-parallel diode, both the transistor and the diode contribute to conduction losses due to their on-state resistance and on-state reverse voltage. These specific parameters can be extracted from the device datasheet and, even though they may exhibit some variation with temperature, they can be treated as constants for the sake of simplification. Considering the on-stated reverse voltage of the transistor as V_s and that of the diode as V_d. Also R_s, and R_d is the transistor and diode internal resistance respectively. The mean conduction losses of the

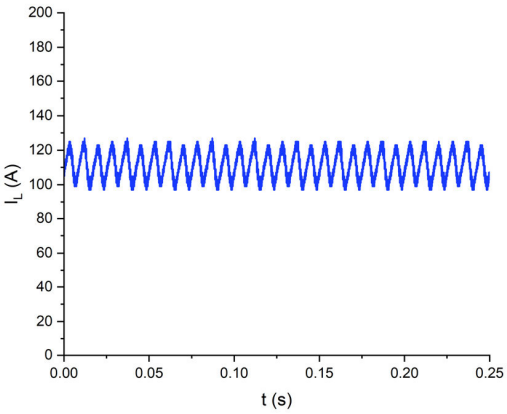

FIGURE 15. The input inductor current of the 10 *kW* SL-SSI system.

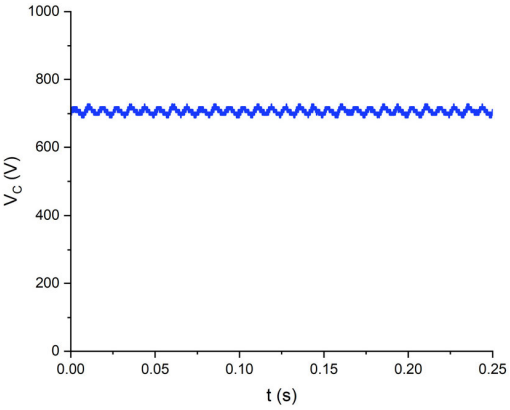

FIGURE 16. The capacitor voltage of the 10 *kW* SL-SSI system.

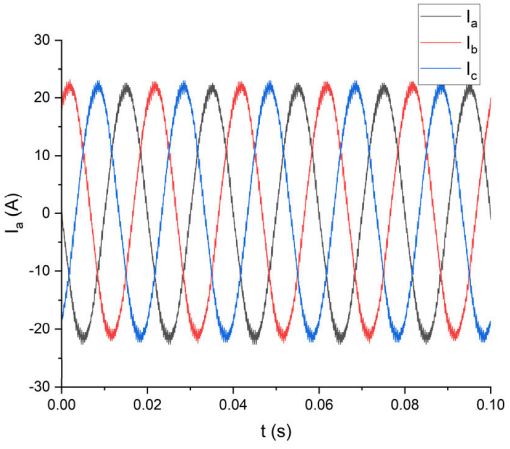

FIGURE 17. The three-phase output current waveforms of the 10 *kW* SL-SSI system.

transistor and diode P^s_{Cond}, P^d_{Cond} can be expressed as

$$P^s_{Cond} = \frac{1}{T}\int_0^T \left(V_s + R_s \cdot i^{\beta}(t)\right) \cdot i(t) \cdot dt \quad (25)$$

$$P^d_{Cond} = \frac{1}{T}\int_0^T \left(V_d + R_d \cdot i^{\beta}(t)\right) \cdot i(t) \cdot dt \quad (26)$$

where T is cycle duration, β is the transistor constant, and $i(t)$ is the current via the transistor or the diode.

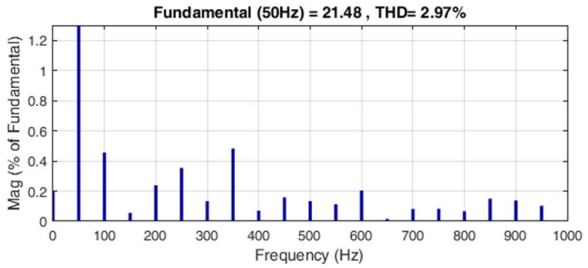

FIGURE 18. The total harmonic distortion (THD) of the SL-SSI output current.

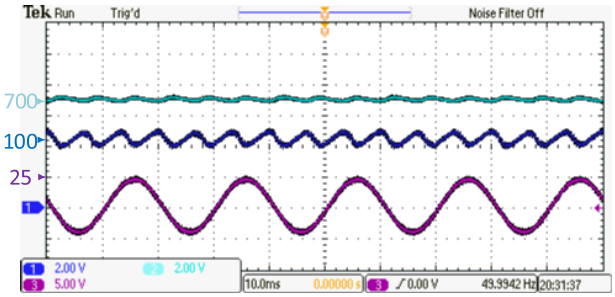

FIGURE 19. The oscilloscope screen of the SL-SSI system.

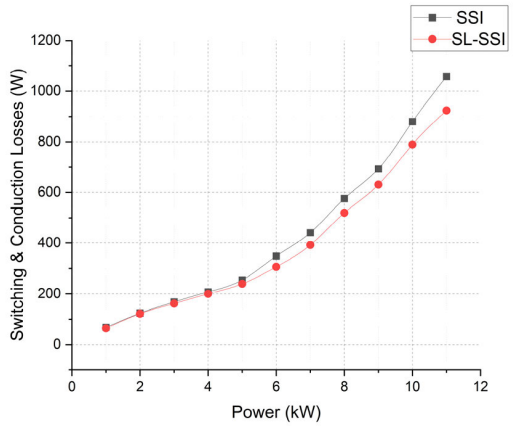

FIGURE 20. The total power losses profiles of the SSI and SL-SSI inverter structures under different load conditions.

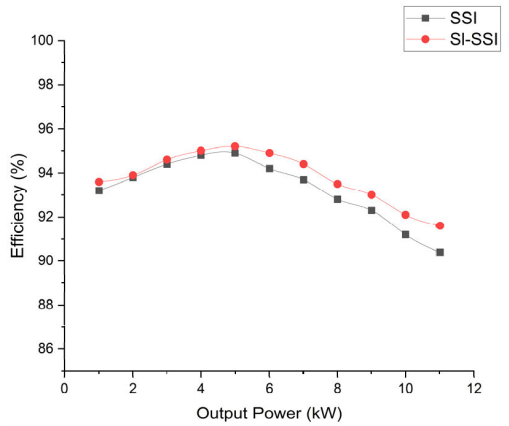

FIGURE 21. Efficiency profiles of the SSI and SL-SSI under load power variation.

The overall conduction losses can be articulated as

$$P_{Cond\_tot} = P^{s}_{Cond} + P^{d}_{Cond} \tag{27}$$

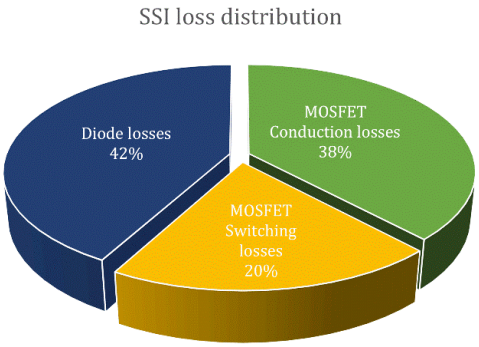

FIGURE 22. Power loss distribution chart of the SSI at 10-kW.

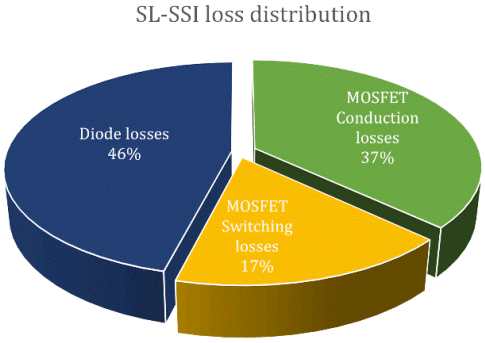

FIGURE 23. Power loss distribution chart of the SL-SSI at 10-kW.

The switching losses represent the dissipated power in each switch and diode throughout the ON and OFF states. These losses can be derived for an individual switch or diode and then extrapolated to encompass the necessary quantity in the proposed Inverters. Supposing a linear variation in voltage and current throughout ON and OFF intervals, the switching losses of the n^{th} switch can be expressed as:

$$P_{ON} = \frac{1}{T}\int_{0}^{tON} v\,(t)\cdot i\,(t)\cdot dt = \frac{1}{6}\cdot V_{switch}\cdot I\cdot t_{ON} \tag{28}$$

$$P_{OFF} = \frac{1}{T}\int_{0}^{tOFF} v\,(t)\cdot i\,(t)\cdot dt = \frac{1}{6}\cdot V_{switch}\cdot I\cdot t_{OFF} \tag{29}$$

where, t_{ON} and t_{OFF} represent the ON and OFF durations, respectively. V_{Switch} and I denote the voltage and current flowing via the switch before and after the ON or OFF actions. Consequently, the comprehensive switching losses can be expressed as:

$$P_{Switch}{}^{s} = \sum_{n^{th}}^{N_{MOSFET}} (P_{ON} + P_{OFF}) \tag{30}$$

where, N_{MOSFET} represents the necessary quantity of MOSFETs in the inverter. The switching losses in diodes are neglected as diodes are considered soft switching devices.

The average total losses of the inverter is

$$P_{Loss\_tot} = P_{Cond\_tot} + P^{s}_{Switch} \tag{31}$$

TABLE 5. Comparison between three-phase SSI topology and three-phase SL-SSI.

Topology	The standard three-phase split source inverter structure	Three-phase Switched-inductor split source inverter structure
Family	Single stage	Single stage
No. of input diodes	**3**	**5**
No. of input inductors	**1**	**2**
No. of input capacitors	1	1
Total inductance in charging states	$\boldsymbol{L}$	$\boldsymbol{2L}$
Total inductance in discharging states	$\boldsymbol{L}$	$\boldsymbol{\frac{L}{2}}$
Average duty cycle	$D_{avg} = \frac{3\sqrt{3}}{4\pi}M + \frac{1}{2}$	$D_{avg} = \frac{3\sqrt{3}}{4\pi}M + \frac{1}{2}$
Boost factor	$\boldsymbol{B = \frac{1}{1-D}}$	$\boldsymbol{B_{SL} = \frac{1+D}{1-D}}$
Overall gain	$\boldsymbol{g = \frac{2\pi . M}{2\pi - 3\sqrt{3}\,M}}$	$\boldsymbol{g_{SL} = \frac{M}{2} \cdot \frac{6\pi + 3\sqrt{3}\,M}{2\pi - 3\sqrt{3}\,M}}$

TABLE 6. Comparison between a 10 kW SSI system and a 10 kW SL-SSI system.

System	SSI	SL-SSI
Input DC-source	100 V	**50 V**
Capacitor	1200 μF	1200 μF
Inductor/s	8 mH	$\boldsymbol{L_a = L_b = 3.5\ mH}$
The DC-link voltage	714.6 V	701.3 V
Output phase voltage	220 V	220 V
Average duty cycle	0.8708	0.8669
Boost factor	7.146	**14.026**
Overall gain	3.11	**9.575**
Carrier frequency	2500 HZ	2500 HZ
Fundamental frequency	50 HZ	50 HZ
Total Harmonic Distortion (THD) of the	3.45%	**2.97%**
Efficiency	91.2%	**92.1%**

Using the above equations and implementing them on both proposed configuration at each switching state in different load conditions, the average power loss and efficiency of the inverters can be calculated as depicted in Fig. 19 and Fig. 20 respectively. The figures depicts a slight advantage for SL-SSI over SSI in total power losses. The detailed losses for SSI and SL-SSI are depicted in Fig. 22 and Fig. 23 respectively.

V. COMPARATIVE STUDY

This section provides a comparative analysis between the conventional SSI and SL-SSI same power rating and using SPWM considering the number of diodes, inductors, capacitors, total inductance during charging and discharging states, average duty cycle, boosting factor, and voltage gain, respectively, as listed in Table 5. Obviously, the conventional SSI structure shows reduced diodes and input passive components

number, however, it offers a reduced boosting factor compared to the SL-SSI. In addition, the inductance of the SSI input inductor is higher than that of the SL-SSI, which reduces the inverter footprint. The numerical comparison between the SSI and SL-SSI structures considering the same power ratings (10-kW) is portrayed in Table 6. Ultimately, the former comparison confirms the efficacy of the single-stage, 3, SL-SSI structure for high boosting factor and small-size applications.

VI. CONCLUSION

This paper introduces an analytical study and comparison of the split source and Switched-inductor split source inverter structures (SSI & SL-SSI). Hence, it compares the former structures considering the rated power of 10 kW systems and using sinusoidal pulse-width modulation (SPWM). In addition, this paper studied the design procedures of both inverters, mathematical modelling, and loss modelling of both structures considering the same power rating. Moreover, the former systems have been implemented using Opal-RT OP4510 and the results coincide with the theoretical and predicted calculations. The comparison shows that the SL-SSI offers a comparatively higher voltage boosting capability, and enhanced power quality operation compared to the SSI. On the other side, the SSI structure shows a reduced passive elements number and reduced ripple in the total input current compared to the SL-SSI.

REFERENCES

[1] H. Abu-Rub, M. Malinowski, and K. Al-Haddad, *Power Electronics for Renewable Energy Systems, Transportation and Industrial Applications*. Hoboken, NJ, USA: Wiley, 2014.

[2] O. Kukrer, S. Bayhan, and H. Komurcugil, "Model-based current control strategy with virtual time constant for improved dynamic response of three-phase grid-connected VSI," *IEEE Trans. Ind. Electron.*, vol. 66, no. 6, pp. 4156–4165, Jun. 2019.

[3] H. Komurcugil, O. Kukrer, and A. Doganalp, "Optimal control for single-phase UPS inverters based on linear quadratic regulator approach," in *Proc. Int. Symp. Power Electron., Electr. Drives, Autom. Motion (SPEEDAM)*, May 2006, pp. 1137–1142.

[4] D. G. Montoya, C. A. Ramos-Paja, and R. Giral, "Improved design of sliding-mode controllers based on the requirements of MPPT techniques," *IEEE Trans. Power Electron.*, vol. 31, no. 1, pp. 235–247, Jan. 2016.

[5] Y. Wang and B. Ren, "Fault ride-through enhancement for grid-tied PV systems with robust control," *IEEE Trans. Ind. Electron.*, vol. 65, no. 3, pp. 2302–2312, Mar. 2018.

[6] M.-K. Nguyen, Y.-C. Lim, and S.-J. Park, "A comparison between single-phase quasi-Z-source and quasi-switched boost inverters," *IEEE Trans. Ind. Electron.*, vol. 62, no. 10, pp. 6336–6344, Oct. 2015.

[7] M. Azizi, O. Husev, and D. Vinnikov, "Single-stage buck–boost inverters: A state-of-the-art survey," *Energies*, vol. 15, no. 5, p. 1622, Feb. 2022, doi: 10.3390/en15051622.

[8] M. Mohr, W. T. Franke, B. Wittig, and F. W. Fuchs, "Converter systems for fuel cells in the medium power range—A comparative study," *IEEE Trans. Ind. Electron.*, vol. 57, no. 6, pp. 2024–2032, Jun. 2010.

[9] Y. P. Siwakoti, F. Z. Peng, F. Blaabjerg, P. C. Loh, and G. E. Town, "Impedance-source networks for electric power conversion—Part I: A topological review," *IEEE Trans. Power Electron.*, vol. 30, no. 2, pp. 699–716, Feb. 2015. [Online]. Available: https://ieeexplore.ieee.org/abstract/document/6778014/

[10] Y. P. Siwakoti, F. Z. Peng, F. Blaabjerg, P. C. Loh, G. E. Town, and S. Yang, "Impedance-source networks for electric power conversion—Part II: Review of control and modulation techniques," *IEEE Trans. Power Electron.*, vol. 30, no. 4, pp. 1887–1906, Apr. 2015.

[11] O. Ellabban and H. Abu-Rub, "Z-source inverter: Topology improvements review," *IEEE Ind. Electron. Mag.*, vol. 10, no. 1, pp. 6–24, Mar. 2016.

[12] F. Z. Peng, "Z-source inverter," in *Proc. Conf. Rec. IAS Annu. Meeting (IEEE Ind. Appl. Soc.)*, vol. 2, May 2002, pp. 775–781, doi: 10.1002/047134608x.w8348.

[13] J. Anderson and F. Z. Peng, "Four quasi-Z-source inverters," in *Proc. IEEE Power Electron. Spec. Conf.*, Jun. 2008, pp. 2743–2749, doi: 10.1109/PESC.2008.4592360.

[14] J. Anderson and F. Z. Peng, "A class of quasi-Z-source inverters," in *Proc. IEEE Ind. Appl. Soc. Annu. Meeting*, Oct. 2008, pp. 1–7, doi: 10.1109/08ias.2008.301.

[15] A. Abdelhakim, P. Mattavelli, and G. Spiazzi, "Three-phase split-source inverter (SSI): Analysis and modulation," *IEEE Trans. Power Electron.*, vol. 31, no. 11, pp. 7451–7461, Nov. 2016, doi: 10.1109/TPEL.2015.2513204.

[16] A. Abdelhakim, P. Mattavelli, and G. Spiazzi, "Split-source inverter," in *Proc. IECON 41st Annu. Conf. IEEE Ind. Electron. Soc.*, Nov. 2015, pp. 1288–1293, doi: 10.1109/IECON.2015.7392278.

[17] A. Abdelhakim, P. Mattavelli, P. Davari, and F. Blaabjerg, "Performance evaluation of the single-phase split-source inverter using an alternative DC–AC configuration," *IEEE Trans. Ind. Electron.*, vol. 65, no. 1, pp. 363–373, Jan. 2018, doi: 10.1109/TIE.2017.2714122.

[18] A. Abdelhakim, P. Mattavelli, and G. Spiazzi, "Three-level operation of the split-source inverter using the flying capacitors topology," in *Proc. IEEE 8th Int. Power Electron. Motion Control Conf. (IPEMC-ECCE Asia)*, May 2016, pp. 223–228, doi: 10.1109/IPEMC.2016.7512289.

[19] A. Abdelhakim, P. Mattavelli, and G. Spiazzi, "Three-phase three-level flying capacitors split-source inverters: Analysis and modulation," *IEEE Trans. Ind. Electron.*, vol. 64, no. 6, pp. 4571–4580, Jun. 2017, doi: 10.1109/TIE.2016.2645501.

[20] A. Abdelhakim and P. Mattavelli, "Analysis of the three-level diode-clamped split-source inverter," in *Proc. IECON 42nd Annu. Conf. IEEE Ind. Electron. Soc.*, Oct. 2016, pp. 3259–3264, doi: 10.1109/IECON.2016.7793581.

[21] S. S. Lee and Y. E. Heng, "Improved single-phase split-source inverter with hybrid quasi-sinusoidal and constant PWM," *IEEE Trans. Ind. Electron.*, vol. 64, no. 3, pp. 2024–2031, Mar. 2017, doi: 10.1109/TIE.2016.2624724.

[22] S. S. Lee, A. S. T. Tan, D. Ishak, and R. Mohd-Mokhtar, "Single-phase simplified split-source inverter (S3I) for boost DC–AC power conversion," *IEEE Trans. Ind. Electron.*, vol. 66, no. 10, pp. 7643–7652, Oct. 2019, doi: 10.1109/TIE.2018.2886801.

[23] Y. Elthokaby, I. Abdelsalam, N. Abdel-Rahim, and I. Mohamed, "Standalone PV-based single-phase split-source inverter using model-predictive control," *Alexandria Eng. J.*, vol. 62, pp. 357–367, Jan. 2023.

[24] C. Yin, W. Ding, L. Ming, and P. C. Loh, "Single-stage active split-source inverter with high DC-link voltage utilization," *IEEE Trans. Power Electron.*, vol. 36, no. 6, pp. 6699–6711, Jun. 2021, doi: 10.1109/TPEL.2020.3038688.

[25] X. Fang, W. Zhang, X. Kan, and Q. Wang, "Three-phase split delta-source inverter: Operating principles and modulation," in *Proc. IEEE 3rd Student Conf. Electr. Mach. Syst. (SCEMS)*, Dec. 2020, pp. 775–780, doi: 10.1109/SCEMS48876.2020.9352323.

[26] M. A. Ismeil, A. Abdelaleem, M. Nasrallah, and E. E. M. Mohamed, "Performance analysis of a novel high gain three-phase split source inverter," in *Proc. 23rd Int. Middle East Power Syst. Conf. (MEPCON)*, Dec. 2022, pp. 1–6, doi: 10.1109/MEPCON55441.2022.10021782.

[27] K. P. Remya, J. Mathew, and V. S. Nandana, "High gain switched inductor-capacitor split source inverter," in *Proc. IEEE 2nd Int. Conf. Smart Technol. Power, Energy Control (STPEC)*, Dec. 2021, pp. 1–5, doi: 10.1109/STPEC52385.2021.9718746.

[28] M. Zhu, K. Yu, and F. L. Luo, "Switched inductor Z-source inverter," *IEEE Trans. Power Electron.*, vol. 25, no. 8, pp. 2150–2158, Aug. 2010, doi: 10.1109/TPEL.2010.2046676.

[29] D. Li, P. C. Loh, M. Zhu, F. Gao, and F. Blaabjerg, "Generalized multi-cell switched-inductor and switched-capacitor Z-source inverters," *IEEE Trans. Power Electron.*, vol. 28, no. 2, pp. 837–848, Feb. 2013, doi: 10.1109/TPEL.2012.2204776.

[30] M. Ismeil, R. Kennel, and H. Abu-Rub, "Modeling and experimental study of three-phase improved switched inductor Z-source inverter," *EPE J.*, vol. 24, no. 4, pp. 14–27, Dec. 2014, doi: 10.1080/09398368.2014.11755455.

[31] M.-K. Nguyen, Y.-C. Lim, and G.-B. Cho, "Switched-inductor quasi-Z-source inverter," *IEEE Trans. Power Electron.*, vol. 26, no. 11, pp. 3183–3191, Nov. 2011, doi: 10.1109/TPEL.2011.2141153.

[32] M.-K. Nguyen, Y.-C. Lim, and J.-H. Choi, "Two switched-inductor quasi-Z-source inverters," *IET Power Electron.*, vol. 5, no. 7, pp. 1017–1025, Aug. 2012, doi: 10.1049/iet-pel.2011.0297.

MOHAMED A. ISMEIL (Member, IEEE) was born in Qena, Egypt, in October 1977. He received the B.Sc. and M.Sc. degrees in electrical engineering from South Valley University, in 2002 and 2008, respectively, and the Ph.D. degree from the Channel System Program, Aswan University, in April 2014. From October 2010 to January 2013, he was a Ph.D. Student with the Department of Electrical Drive Systems and Power Electronics, Technical University of Munich, Germany. From April 2014 to September 2018, he was an Assistant Professor with Aswan Faculty of Engineering, Aswan University. Since October 2018, he has been an Associate Professor with Qena Faculty of Engineering, South Valley University. From March 2020 to November 2022, he was the Head of the Electrical Department, Qena Faculty of Engineering. He is an Associate Professor with the College of Engineering, King Khalid University, Saudi Arabia. His current research interests focus on power electronics applications in wind energy conversion systems, PV interface with the utility, smart grid technologies, and digital control applications (PIC, FPGA, and DSP). His main interest is power inverter design for renewable applications.

AHMED ABDELALEEM was born in Qena, Egypt, in 1996. He received the B.Sc. degree in electrical engineering from South Valley University, Qena, in 2019, where he is currently pursuing the master's degree with the Department of Electrical Engineering, Faculty of Engineering. He is also a Teaching Assistant with South Valley University. His current research interests include power electronic converters and renewable energy systems.

AHMED ISMAIL M. ALI (Member, IEEE) was born in Qena, Egypt, in 1991. He received the B.Sc. and M.Sc. degrees in electrical engineering from the Faculty of Engineering and Technology, South Valley University, Qena, in 2013 and 2017, respectively, and the Ph.D. degree in electrical engineering from Nagoya Institute of Technology, Nagoya, Japan, in 2022. Since 2013, he has been with the Department of Electrical Engineering, Faculty of Engineering, South Valley University, as an Administrator and a Research Assistant, since 2017, where he is currently an Assistant Professor with the Department of Electrical Engineering. His research interests include power electronic converters, PWM techniques, dc/ac and ac/dc converters, modular multilevel converters (MMxC), control systems, and renewable energy applications, in addition to battery chargers for electric vehicle applications. He received the South Valley University Prize for International Publishing, in 2018 and 2023.

M. NASRALLAH was born in Qena, Egypt, in 1987. He received the B.Sc. degree in electrical engineering from the High Institute of Energy, South Valley University, Egypt, in 2008, and the M.Sc. and Ph.D. degrees from the Department of Electrical Engineering, Faculty of Engineering, South Valley University, in 2013 and 2021, respectively. He is currently an Assistant Professor with the Department of Electrical Engineering, Faculty of Engineering, South Valley University. His current research interests include smart grids and renewable energy systems.

HANY S. HUSSEIN (Senior Member, IEEE) received the B.Sc. degree in electrical engineering and the M.Sc. degree in communication and electronics from South Valley University, Egypt, in 2004 and 2009, respectively, and the Ph.D. degree in communication and electronics engineering from Egypt–Japan University of Science and Technology (E-JUST), in 2013. In 2012, he was a special Researcher Student with Kyushu University, Japan. He has been an Associate Professor with the Faculty of Engineering, Aswan University, since 2019. He is currently an Assistant Professor with the College of Engineering, King Khalid University, Saudi Arabia. His research interests include digital signal processing for communications, multimedia, image, video coding, and low-power wireless communications. He is a technical committee member of many international conferences and a reviewer of many international conferences, journals, and transactions. He was the General Co-Chair of the IEEE ITCE, in 2018.

ESSAM E. M. MOHAMED (Member, IEEE) was born in Qena, Egypt, in 1974. He received the B.Sc. and M.Sc. degrees in electrical power and machines engineering from the Faculty of Energy Engineering, Aswan University, Aswan, Egypt, in 1997 and 2003 respectively, and the Ph.D. degree in electrical engineering from the University of Sheffield, Sheffield, U.K., in 2011. In 1999, he joined the Department of Electrical Engineering, Faculty of Energy Engineering, Aswan University. Since 2013, he has been with the Department of Electrical Engineering, Faculty of Engineering, South Valley University, Qena. His research interests include power electronics, electrical machine design and control, electric drives, and renewable energy systems. He is a Founder and the Manager of the South Valley University IEEE Student Branch.